Optical design of a near-infrared birefringent filter system and measurement of birefringent index of calcite at 1.56 μm

Jingshan Wang, MEMBER SPIE
Haimin Wang
New Jersey Institute of Technology
Department of Physics
Newark, New Jersey 07102
and
New Jersey Institute of Technology
Big Bear Solar Observatory
40386 North Shore Lane
Big Bear City, California 92314

Thomas J. Spirock
New Jersey Institute of Technology
Big Bear Solar Observatory
40386 North Shore Lane
Big Bear City, California 92314
and
New Jersey Institute of Technology
Department of Electrical and Computer Engineering
Newark, New Jersey 07102

Chik-Yin Lee
The Chinese University of Hong Kong
Department of Physics
Shatin, New Territories
Hong Kong

Nuggehalli M. Ravindra, MEMBER SPIE
New Jersey Institute of Technology
Department of Physics
Newark; New Jersey 07102

Jun Ma
New Jersey Institute of Technology
Big Bear Solar Observatory
40386 North Shore Lane
Big Bear City, California 92314

Philip R. Goode
New Jersey Institute of Technology
Department of Physics
Newark, New Jersey 07102
and
New Jersey Institute of Technology
Big Bear Solar Observatory
40386 North Shore Lane
Big Bear City, California 92314

Carsten Denker
New Jersey Institute of Technology
Big Bear Solar Observatory
40386 North Shore Lane
Big Bear City, California 92314

Abstract. We present an optical design of a near-IR (at FeI15648.5 Å) birefringent filter system that is used to form a magnetograph to obtain chromatic images of the sun and measure the solar magnetic field at the Big Bear Solar Observatory (BBSO). This magnetograph consists of an interference prefilter, a polarization analyzer, a wavelength-tunable birefringent filter, and a Fabry-Perot Etalon. This system is expected to achieve a clean narrow pass band of 1/8 Å. It can also be tuned across the spectral line to obtain line profiles of 2-D fields of view. During the design of the tunable near-IR birefringent filter and the testing of its components, we found that the value of the birefringent index $\mu(n_e - n_o)$ of calcite at a spectral range near 15648.5 Å is different from the value quoted in the literature. Because the birefringent index is important for the design of optical components, the birefringent index of calcite and its thermal coefficient were measured. Test results of the four pairs of calcite plates used in the birefringent filter are presented. [DOI: 10.1117/1.1367350]

Subject terms: near-infrared; birefringent filter; calcite; birefringent index; Zeeman effect.

Paper 200425 received Oct. 30, 2000; revised manuscript received Jan. 24, 2001; accepted for publication Jan. 24, 2001.

 0091-3286/2001/$15.00

1 Introduction

The study of magnetic fields on the sun is critical to the research of solar phenomena. Narrow passband birefringent filters play a very important role in solar magnetographs, which measure the strength and direction of magnetic fields on the sun. Currently, most magnetographs operate in the wavelength range of visible light[1–4] (from 4000 to 7000 Å). According to the Zeeman effect, the splitting of solar spectral lines, $\Delta\lambda$, which is due to the solar magnetic field, is proportional to $g\lambda^2 B$, where λ is the wavelength of the Zeeman sensitive line, g is the Lande factor of the line, and B is the magnetic field strength. Usually, large sunspots possess strong magnetic fields—on the order of 2000 to 3000 Gauss. However, in other solar features such as plages, the magnetic fields are only about 1000 to 1500 Gauss, and there exist weak, subkilogauss fields in other structures, such as the intranetwork magnetic fields.[5] The Zeeman splitting induced by a subkilogauss field is too small to be measured[6,7] in the visible spectrum. For example, if $\lambda = 5250.2$ Å (with $g = 3.0$) and $B = 1000G$, $\Delta\lambda = 4.7\times10^{-13}$ $g\lambda^2 B = 4.7\times10^{-13}\times3\times5250^2\times1000 \cong 0.039$ Å. However, for a near infrared line, e.g., FeI15648.5 Å (with $g = 3.0$), the Zeeman splitting $\Delta\lambda$ ($\propto g\lambda^2 B$) would be much larger for the same magnetic field. If $B = 1000G$, $\Delta\lambda = 4.7\times10^{-13}$ $g\lambda^2 B = 4.7\times10^{-13}\times3\times15648.5^2\times1000 \cong 0.35$ Å. The Zeeman splitting of an infrared line is almost ten times as that with a visible line with a given B field. Therefore, weaker magnetic field strengths can be more precisely measured using near infrared lines.

It has been shown that magnetic field strengths can be measured as low as 100 Gauss by using the line ratio between FeI15648.5 Å and FeI15652.9 Å lines.[6] FeI15648.5 Å ($e^7D_1 - 3d^6 4s5p^7D_1^0$) is a Zeeman triplet with a Lande factor g of 3 and the strongest spectral line in the H-band. FeI15652.9 Å ($f^7D_5 - (9/2)[7/2]_4^0$) has a Lande factor g of 1.53 and corresponds to a weaker spectral transmission. The use of infrared lines as probes of solar magnetic features has been discussed in detail by Solanki, Rnedi, and Livinston.[8] Therefore, we choose FeI15648.5 Å as the working wavelength of the near-IR filter system to measure the solar magnetic field.

From a technical point of view, the fabrication of an infrared filter system is much more difficult than a similar filter in visible light because testing the IR filter components is not as easy as in the visible. Nevertheless, the enormous technical progress made in recent years on infrared cameras, Fabry-Perot Etalons, and other IR optical components have led to the possibility of adequately testing and fabricating an IR filter system.

We use a near-infrared InGaAs camera built by Sensors Unlimited. This camera is 12 bit, has 320×240 pixels, and is sensitive from 10,000 to 17,000 Å. It is used to test some of the optical components of this IR filter system in addition to near-IR solar observations. This birefringent filter will be used as a prefilter for a Fabry-Perot. In the design of a birefringent filter, the most important parameter is the birefringent index $\mu(n_e - n_o)$ of the calcite. However, the values of μ in the near-infrared region quoted in the literature are not precise enough for applications in optical design. The spectrograph at the Big Bear Solar Observatory (BBSO) was used to measure the birefringent index, at a constant temperature, of a sample calcite crystal and to test the four pairs of calcite that will be used in the actual birefringent filter. We emphasize the measurement of the calcite birefringent index and the design of the entire filter system, especially the birefringent filter. An analysis of the results will be presented and discussed.

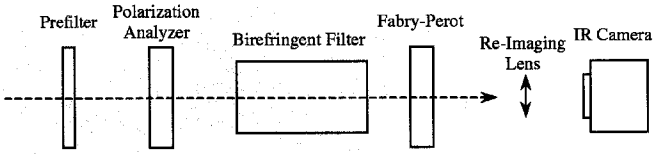

Fig. 1 Scheme of the IR magnetograph.

2 Description of the Magnetograph

A typical magnetograph has three stages: interference prefilter, magnetic analyzer, and a narrow-band filter. The optical scheme of the entire near-IR filter system under construction is presented in Fig. 1. The full-width-half-maximum (FWHM) of the interference prefilter is about 30 Å. The magnetic analyzer is usually an electro-optical modulator, e.g., KDP(KH_2PO_4) or DKDP(KD_2PO_4) crystal. However, these electro-optical modulators are difficult to control because they tend to require high voltages (a few thousands volts). Hence, we have chosen an approach that consists of a quarter waveplate and liquid crystal variable retarder, which is controlled with low voltages as the analyzer.[9] The narrow-band filter is the most important part and is difficult to construct. The requirements for high spectral resolution, high throughput, and tunability have led us to the consideration of a combination of a Fabry-Perot Etalon (narrower passband) and a birefringent filter (wider passband). The birefringent filter, designed below, will be used as a prefilter to eliminate the side bands of the Fabry-Perot.

The Fabry-Perot, being constructed by Queensgate Instruments, has the same specifications as the IR Fabry-Perot currently being used at National Solar Observatory/Sac Peak. The characteristics of the Fabry-Perot have been measured using the horizontal spectrograph (HSG) at NSO/Sac Peak[10] (Table 1). From Table 1, we see that the free spectral range (FSR)— the separation between two maximum values of the passbands— is 5.517 Å and the FWHM of this Etalon is 0.119 Å (about 1/8 Å). These values satisfy the requirement for the proposed IR magnetograph.

Table 1 The measured characteristics of the narrow-band Fabry-Perot at 15231 Å and calculated values at 15648.5 Å[10].

Characteristics	Measured Value at 15231.0 Å	Calculated Value at 15648.5 Å
Plate Separation	22193777 Å	22193777 Å
FWHM	0.113 Å	0.119 Å
Free Spectral	5.225 Å	5.517 Å
Range Finess	46.24	46.36
Transmission	78%	...

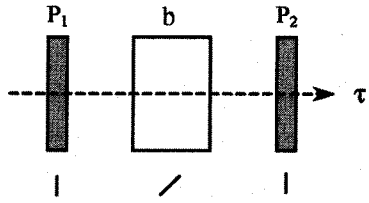

Fig. 2 Principle of the measurement. The | represents polarizer direction along the surface, and / represents the direction of the optical axis along the surface of the calcite plate.

3 Measurement of the Calcite Birefringent Index

3.1 *Principle of Measurements*

If polarized light is passed though a birefringent crystal, e.g., a plate of calcite, with the optical axis z of the crystal parallel to the face and 45 deg to the polarization direction of entrance light, it is split into two rays, the ordinary (o) component and the extraordinary (e) component. The o and e components experience different refractive indices n_o and n_e, respectively. The difference between n_e and n_o, i.e., $\mu(\lambda,T)=n_e-n_o$, is known as the birefringent index and is a function of wavelength λ (dispersion) and temperature T (thermal effects). The value of μ for calcite is negative and positive for quartz (another birefringent crystal). The phase difference δ between the e and o components is given by:

$$\delta=2\pi\frac{(n_e-n_o)d}{\lambda}=2\pi\frac{\mu d}{\lambda}=2\pi\sigma, \tag{1}$$

where d is the thickness of the birefringent crystal, $\sigma=\mu d/\lambda$ is called retardation, and λ is the wavelength of light. If a birefringent crystal b is sandwiched between two parallel polarizers (Fig. 2), the output is the interference pattern of the e and o components, given by:

$$\tau_{\|}=\cos^2\left(\frac{\delta}{2}\right)=\cos^2\left(\frac{\mu d}{\lambda}\pi\right)=\cos^2(\sigma\pi), \tag{2}$$

where τ is the transmission at a particular wavelength λ.

When the retardation $\sigma=\mu d/\lambda$ is an integer, the transmission τ will be maximized, whereas it will be minimized if σ is a half integer. If p is the wavelength separation of two maximum peaks of the transmission at the same temperature T, we have

$$n=\frac{\mu d}{\lambda}, \quad \text{and} \quad n+1=\frac{\mu d}{\lambda+p}\approx\frac{\mu d}{\lambda}\left(1-\frac{p}{\lambda}\right). \tag{3}$$

From Eq. (3), we get

$$n=-\frac{\lambda}{p}, \quad \text{and} \quad \mu=\frac{n\lambda}{d}=-\frac{\lambda^2}{pd}. \tag{4}$$

Therefore, if we can measure p, we can calculate μ using Eq. (4).

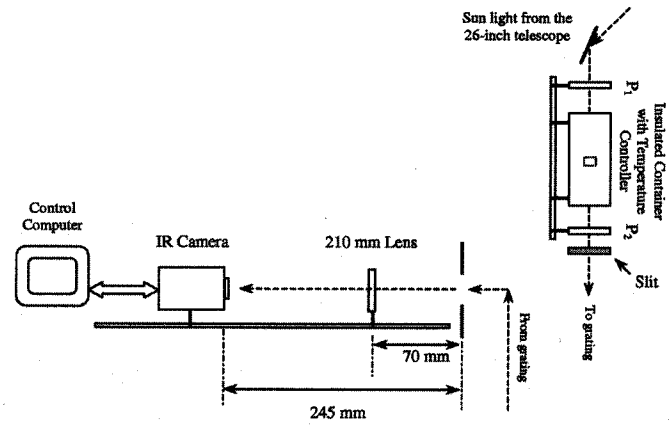

Fig. 3 Setup of the instrument for measuring the calcite birefringent index.

3.2 *Calcite Birefringent Index and Its Thermal Coefficient*

The birefringent index of calcite, $\mu=n_e-n_o$, is a function of wavelength λ and temperature T. Therefore, when measuring μ, the temperature of calcite must be stabilized with a controller (of accuracy ±0.1°C at least). A sample calcite plate with a thickness of $d_0=10498.0\pm3.0\,\mu$m at $T_0=69.0$°F (21.56°C) was used in this measurement. The thermal expansion coefficient along the direction perpendicular to the optical axis of calcite is $\beta=-3.7\times10^{-6}$/K (see Ref. 11).

3.2.1 *Setup of the instrument and the interference images*

Figure 3 shows the setup for the test with the spectrograph at BBSO. First, the two polarizers, P_1 and P_2, are separately mounted on accurate rotators, and are set to be parallel to each other and to one of the inner sides of the insulated container. The sample of calcite is square and the optical axis of the calcite plate is along the surface and 45.0 deg$\pm2'$ to its one side.

The sunlight from the 26-in telescope enters the thermally insulated container and is focused on the slit before being incident on the grating. From the grating, it proceeds to the IR camera and subsequently to the online computer for image acquisition and analysis. We first obtain the spectral image [Fig. 4(j)] for dispersion and wavelength calibration without the calcite inside the container. With the sample of calcite inside the container, the transmission images (interference patterns) at different temperatures (Fig. 4) can be obtained. The interference pattern shifts to a shorter wavelength with increasing temperature due to variations in the birefringent index and thickness of the calcite.

3.2.2 *Birefringent index at room temperature (21°C) and at the filter working temperature (43°C)*

From Fig. 4(j) we can obtain the spectral profile versus pixel position or wavelength λ (Fig. 5). Figure 5 shows a sample spectral profile near FeI15648.5 Å. Two lines L1, L2, whose wavelengths are $\lambda(L1)=15621.695$ Å, $\lambda(L2)=15662.012$ Å, can be seen in the figure. A spectral reso-

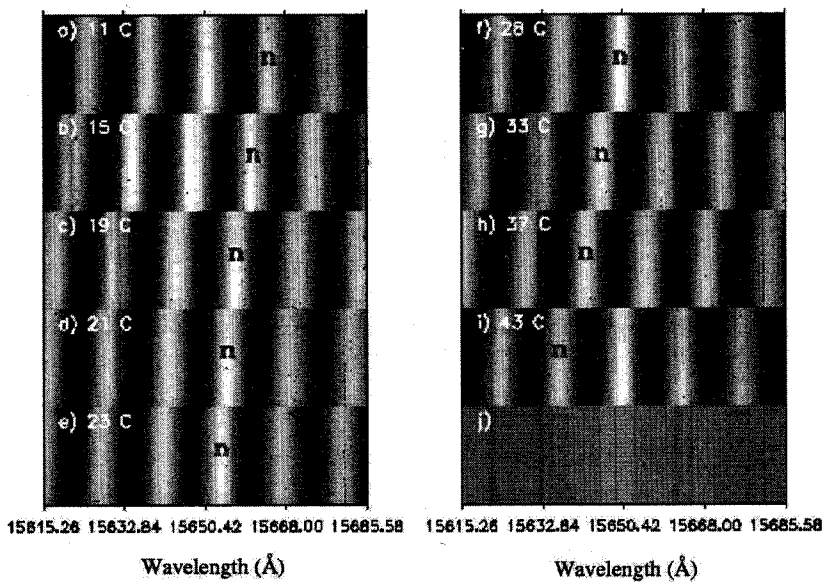

Fig. 4 Transmission images at different temperatures: (a) $T=11°C$, (b) $T=15°C$, (c) $T=19°C$, (d) $T=21°C$, (e) $T=23°C$, (f) $T=28°C$, (g) $T=33°C$, (h) $T=37°C$, (i) $T=43°C$, and (j) spectral image near 15648.5 Å.

lution of 0.2940 Å/pixel is obtained from this data. This resolution results from dividing the spectral range by the number of pixels in the x-axis of the image. Thus, the wavelength corresponding to each pixel may be calculated and the x-axis can be translated into wavelength. Although the background of the images is not uniform, it does not affect the analysis of the data.

Figure 6 is the normalized transmission profiles of the sample calcite with respect to wavelength at room temperature $T=21°C$ and the filter operating temperature $T=43°C$. The separation between the two maximum peaks p is measured as $p(21°C)=13.156$ Å and $p(43°C)=13.176$ Å. Using Eq. (4), we get $n(\lambda=15648.5\ \text{Å}, T=21°C)=-15648.5\ \text{Å}/13.156\ \text{Å}=-1189.4356$ and $n(\lambda=15648.5\ \text{Å}, T=43°C)=-15648.5\ \text{Å}/13.176\ \text{Å}=-1187.6662$. Because the thickness of the calcite is $d(21°C)=d_0(1+\beta\Delta T)=10498.03\ \mu\text{m}$ and $d(43°C)=d_0(1+\beta\Delta T)=10497.18\ \mu\text{m}$, using Eq. (5) we obtain,

$$\mu(\lambda=15648.5\ \text{Å}, T=21°C)=n\lambda/d(21°C)\approx-0.1772989, \tag{5}$$

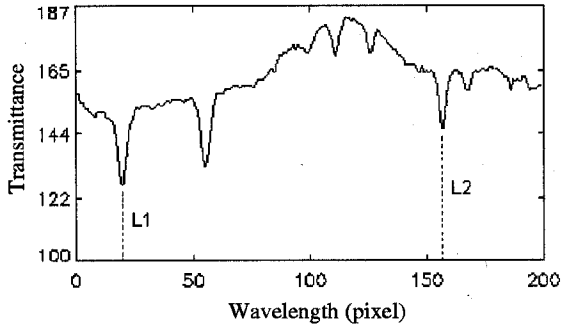

Fig. 5 Spectral profile near FeI15648.5 Å, L_1, L_2 represent the two lines for calibrating the spectral resolution.

$$\mu(\lambda=15648.5\ \text{Å}, T=43°C)=n\lambda/d(43°C)\approx-0.1770494. \tag{6}$$

The accuracy in the measurement of p is about $\Delta p\approx\pm0.03$ Å (0.2940 Å has been approximated to 0.3 Å and the error during data analysis in 0.3 Å/10=0.03 Å) and $\Delta d\approx\pm3.0\ \mu\text{m}$. Therefore, the error in the measurement of μ is:

$$\Delta\mu\approx\mu(\Delta p/p+\Delta d/d)\approx\pm4.5\times10^{-4}. \tag{7}$$

Thus,

$$\mu(\lambda=15648.5\ \text{Å}, T=21°C)\approx-0.17730\pm4.5\times10^{-4}, \tag{8}$$

$$\mu(\lambda=15648.5\ \text{Å}, T=43°C)\approx-0.17705\pm4.5\times10^{-4}. \tag{9}$$

3.2.3 *Thermal coefficients of the birefringent index*

Although we determined the birefringent index of calcite at $T=21°C$ and $T=43°C$, we could not calculate the thermal coefficient of μ using these indices because of the measurement error. In this section, the thermal coefficients of calcite are measured independent of the birefringent index μ and thickness of the sample. Figure 4 clearly shows the shifts to the blue (short wavelength) end of the spectrum for the maximum peaks with an increase in temperature. These shifts are due to the variation of μ and shrinking of the calcite thickness as temperature increases. If α is the thermal coefficient of μ, and β is the thermal expansion coefficient, we have

$$\mu(T_2)\approx\mu(T_1)(1+\alpha\Delta T), \tag{10}$$

and

$$d(T_2)\approx d(T_1)(1+\beta\Delta T), \tag{11}$$

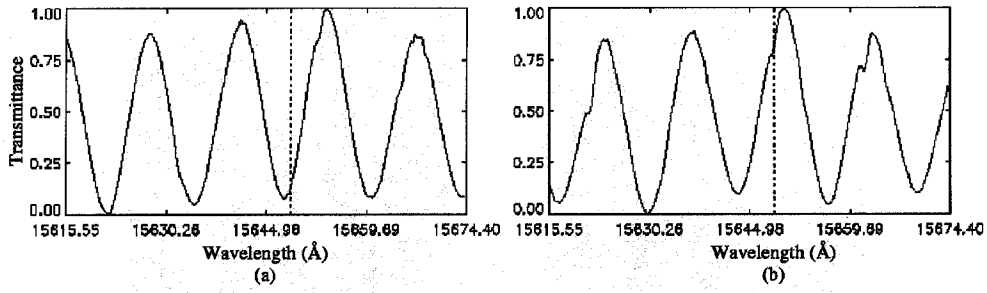

Fig. 6 The normalized transmission profiles of the sample calcite at (a) $T=21°C$ and (b) $T=43°C$. The dashed lines indicate the FeI15648.5 Å line.

where $\Delta T=T_2-T_1$, $\beta=-3.7\times10^{-6}/K$. The higher orders of ΔT are ignored.

For a specific peak of intensity, let the retardation be n at a specific temperature T_1 and let the position be λ_1 as shown in Fig. 4. The position of the peak will shift from λ_1 to λ_2 as the temperature increases, where $\Delta\lambda=\lambda_2-\lambda_1$. Therefore, we have

$$\text{at } T_1, \quad n=\frac{\mu_1 d_1}{\lambda_1}, \tag{12}$$

$$\text{at } T_2, \quad n=\frac{\mu_2 d_2}{\lambda_2}\approx\frac{\mu_1(1+\alpha\Delta T)d_1(1+\beta\Delta T)}{\lambda_1+\Delta\lambda}$$

$$\approx\frac{\mu_1 d_1}{\lambda_1}\left(1+\alpha\Delta T+\beta\Delta T-\frac{\Delta\lambda}{\lambda_1}\right). \tag{13}$$

The higher order terms are neglected in Eq. (13). Combining Eqs. (12) and (13), we obtain

$$\alpha+\beta=\frac{\Delta\lambda}{\lambda_1\Delta T}. \tag{14}$$

Knowing the wavelengths at which the peaks occur (marked as n in Fig. 4) and with the use of Eq. (14), we get the results for α as shown in Table 2. The α is obtained by subtracting β from values of $\alpha+\beta$. The thermal coefficient, α, and the thermal expansion coefficient, β, are properties of calcite that are independent of the thickness of the crystal and its birefringent index.

Table 2 Measurement results for the thermal coefficient of the birefringent index.

Temperature (°C)	Wavelength at peak n (Å)	$\alpha+\beta$ (10^{-5}/°C)	α (10^{-5}/°C)
11.3	15664.768	−5.69	−5.32
15.2	15661.293	−5.81	−5.51
19.2	15657.494	−5.85	−5.48
21.2	15655.727	−5.97	−5.60
23.0	15653.952	−5.78	−5.41
28.0	15649.833	−5.23	−4.86
33.0	15645.772	−5.49	−5.12
37.0	15642.153	−5.93	−5.56
43.0	15636.444	−6.08	−5.71
		Average:	−5.37

The values in Table 2 show some variation of α with respect to temperature. The average value of α is about -5.37×10^{-5}. We use this value to get the birefringent index of calcite at 43°C,

$$\mu(43°C)\approx\mu(21°C)[1.0+(43.0°C-21.2°C)\times(-5.37\times10^{-5}/°C)]\approx-0.17709. \tag{15}$$

This value of μ at 43°C matches quite well with the value obtained in Eq. (9). Note that the values of α in Table 2 are in accordance with the data reported in the literature.[12]

4 Optical Design of the Near-IR Birefringent Filter

Birefringent filters first began to be used in solar instruments in the 1930s.[13] Usually, a birefringent filter includes several elements. One element consists of a birefringent crystal plate sandwiched between two parallel or crossed linear polarizers. If there is a sequence of elements, each containing a birefringent crystal plate with half the thickness of the previous element, a birefringent filter is formed. In 1949, Evans developed the "wide field" configuration to reduce the retardation error due to the field of view caused by the nonnormal incidence of light.[14] This method has been widely used in the design of a variety of birefringent filters. In a birefringent filter with the "wide field" configuration, the calcite plate is split into two equally thick parts and a half waveplate is sandwiched between them.

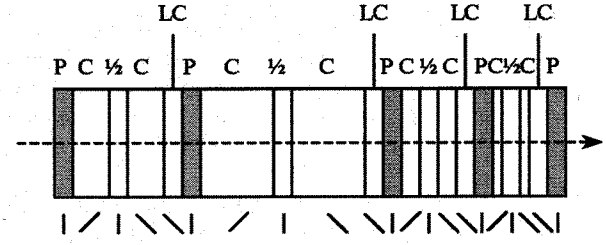

Fig. 7 Scheme of the optical design of the near-IR birefringent filter: P=polarizer, C=calcite, 1/2=wide-field half waveplate, and LC =liquid crystal variable retarder. The | represents polarization direction of the polarizers or the direction of optical axis of the 1/2 waveplates, / or \ represents the direction of the optical axis of the calcite plate or the liquid crystal retarder.

Table 3 Design parameters of the birefringent filter.

Element #	FWHM(Å)	Material	Thickness (mm)	Retardations	Field of View	Shape/Size
1	2.5	Calcite	13.838×2	3128	Wide	Octagon/37.00×37.00 mm
2	5.0	Calcite	6.912×2	1564	Wide	Octagon/37.00×37.00 mm
3	10.0	Calcite	3.460×2	782	Wide	Octagon/37.00×37.00 mm
4	20.0	Calcite	1.730×2	391	Wide	Octagon/37.00×37.00 mm
Waveplate	—	Quartz	2.00~3.00 mm	$\frac{1}{2}$	—	Octagon/37.00×37.00 mm
Polarizer	—	Corning, Inc	2.00~3.00 mm	—	—	—

4.1 *Scheme of the Optical Design of the Near-IR Birefringent Filter*

In the design of our near-IR birefringent filter, we use the wide field configuration. Liquid crystal variable retarders are used to tune the passband of the filter. Figure 7 shows a scheme of the optical design of the near-IR birefringent filter.

The linear polarizers are parallel to each other. This filter includes four elements: d_1, $d_2=d_1/2$, $d_3=d_1/4$, $d_4=d_1/8$. The transmission τ of this filter is given by:

$$\tau=\cos^2\left(\pi\frac{\mu d_1}{\lambda}+\Delta_1\right)\cos^2\left(\pi\frac{\mu d_2}{\lambda}+\Delta_2\right)\times\cos^2\left(\pi\frac{\mu d_3}{\lambda}+\Delta_3\right)\cos^2\left(\pi\frac{\mu d_4}{\lambda}+\Delta_4\right), \quad (16)$$

where Δ_i, $i=1,2,3,4$, are the phase differences given by the liquid crystal variable retarders to shift the wavelength of the passband within a period in every element.

Because the free spectral range of the Fabry-Perot Etalon is about 5.5 Å, the FWHM of the narrowest element in this infrared birefringent filter must be less than 5.5 Å to properly eliminate the side peaks of the Fabry-Perot. To reduce the side band effect, the FWHM of the narrowest element of the filter must be approximately 2.5 Å. In Table 3, the design parameters of the filter are presented.

This birefringent filter is designed to be tunable so that the passband can cover the two magnetically sensitive lines at FeI15648.5 Å ($g=3$) and FeI15652.8 Å ($g=1.53$). An advantage of a tunable filter is that the wavelength of the passband can be easily calibrated and we can use both lines to measure magnetic fields.

4.2 *Half Waveplates*

The half waveplates are used for the wide-field configuration elements. Using the equation $\mu d_{1/2}/\lambda=1/2$, we obtain the thickness of a zero-order half waveplate for quartz as the material of choice,

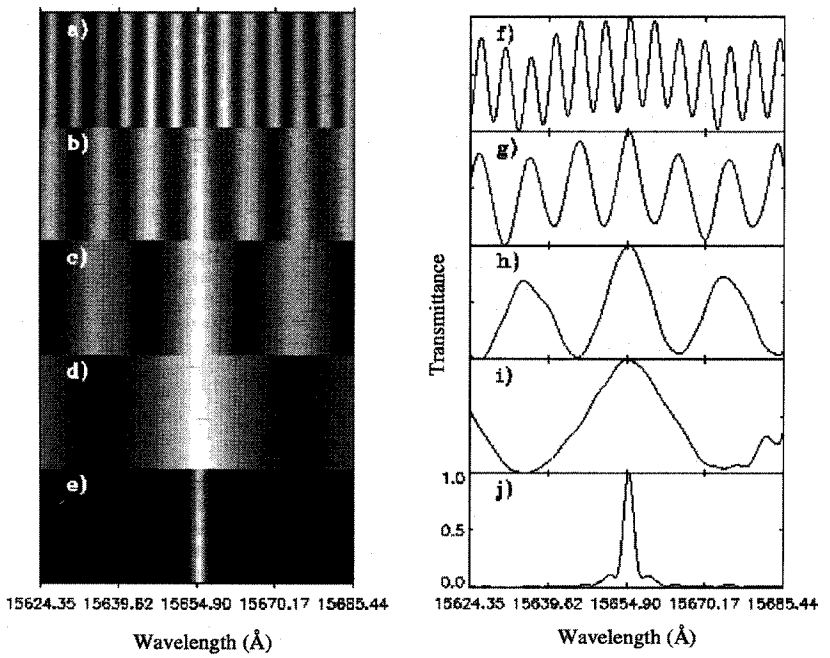

Fig. 8 Transmission image of each pair of calcite and simulated passband of the near-IR birefringent filter: (a) through (d) transmission images of the calcite elements; (f) through (i) normalized profiles of the transmission images; (e) simulated passband of the filter [product of image (a), (b), (c), and (d)], and (j) normalized simulation profile of the passband of the filter.

Table 4 Measurement results for every pair of calcite used in the near-IR birefringent filter.

Transmission image	Separation between two peaks (Å)	FWHM (Å)
(a)	4.813	2.407
(b)	9.630	4.815
(c)	19.13	9.565
(d)	38.52	19.26
Simulated passband of filter	—	2.254

$$d_{1/2}=\frac{\lambda}{2\mu_q}=\frac{15648.5\times10^{-7}\,\text{mm}}{2\times0.00879}\approx0.089\,\text{mm}. \quad (17)$$

From mechanical considerations, the numerical value of $d_{1/2}$ in Eq. (15) is very small. We can design the waveplate consisting of two crossed quartz plates with a thickness difference between them of 0.089 mm, i.e., $\Delta d=d_1-d_2=d_{1/2}$. The optical axis of the waveplate will be along that of the thicker plate.

4.3 *Testing the Four Pairs of Calcite with the Spectrograph*

We tested the four pairs of calcite that to be used in the IR birefringent filter on the spectrograph of BBSO. The setup of the instrument is the same as in Fig. 3. The working temperature is set to 43.0°C with an accuracy ±0.1°C. Polarizer P_1 is parallel to P_2 and a half waveplate is sandwiched between a pair of calcite crystals just as in the wide-field configuration.

The test results shown in Fig. 8 show the transmission image of the elements 1. (d_1), 2. (d_2), 3. (d_3), and 4. (d_4), respectively. To simulate the passband of the filter, we shift Figs. 8(a), 8(c), and 8(d) slightly to align the peaks. This task will be performed by the liquid crystal variable retarders in the working filter. In Table 4, the experimentally measured values are listed and these are the average between the peaks near FeI15648.5 Å. The FWHM of the near-IR filter is approximately 2.254 Å.

The data in Table 4, obtained from testing and the simulated passband profile of the birefringent filter [in Fig. 8(j)], show that the thickness of the four calcite pairs are matched to each other and will perform to our desired specifications of the filter. Due to the nonuniformity in the brightness of the background on the images, the value of the lowest intensity in Figs. 8(f) and 8(g) are not equal to zero. Therefore, the side band in Fig. 8(j) is slightly higher than that in the theoretical case. When the pairs of calcite crystal are used in the construction of the actual near-IR birefringent filter, and the filter is used in the uniform light beam of a telescope, the side bands should be reduced to lower values.

5 Conclusions

We have designed a near-IR birefringent filter for the measurement of the solar magnetic field at BBSO. The four pairs of calcite elements used in this filter were completely polished and tested on the spectrograph at BBSO. The test results show that the calcite and half waveplates at 15648.5 Å have good qualities for fabricating the birefringent filter. This filter is being fabricated by Cambridge Research & Instrument, Inc., Boston.

To design the near-IR birefringent filter, we measured the birefringent index of calcite at 15648.5 Å and its thermal coefficient: $\mu(\lambda=15648.5\ \text{Å}, T=21°\text{C})\approx-0.17730\pm4.5\times10^{-4}$, at room temperature, $\mu(\lambda=15648.5\ \text{Å}, T=43°\text{C})\approx-0.17705\pm4.5\times10^{-4}$, at working temperature of the near-IR filter,

$$\alpha\approx-5.37\times10^{-5}/°\text{C}.$$

Although the error in μ looks slightly larger than desired, it is good enough to be applicable in the design of the optical components of the calcite crystal near 15648.5 Å.

Acknowledgments

We would like to thank the staff of the Big Bear Solar Observatory for their support and suggestions during the tests, especially Jeff Nenow, Randy Fear, Bill Marquette, and Owen Phairis. The authors would like to thank the referees for their helpful comments and suggestions.

References

1. J. M. Beckers, L. Dickson, and R. S. Joyce, "A fully tunable Lyot-Ohman filter," AFCRL-TR-75-0090 (1975).
2. J. S. Wang, G. Ai, G. Song, B. Zhang, X. Ye, Y. Nie, T. Chieveh, W. Tsay, and H. Li, "Universal birefringent filter with a new double passband mode," *Sol. Phys.* **161**, 229–239 (1995).
3. D. Bonaccini, F. Cavallini, G. Ceppatelli, and A. Righini, "High resolution solar bidimensional spectroscopy with a universal birefringent filter in tandem with a Fabry-Perot interferometer," *Astron. Astrophys.* **217**, 368–374 (1989).
4. D. Bonaccini and F. Stauffer, "High resolution solar bidimensional spectroscopy with a universal birefringent filter in tandem with a Fabry-Perot interferometer: tests and experimental results," *Astron. Astrophys.* **229**, 272–278 (1990).
5. H. Lin, "On the distribution of the solar magnetic fields," *Astrophys. J.* **446**, 421–430 (1995).
6. D. Rabin, "Spatially extended measurements of magnetic field strength in solar plages," *Astrophys. J.* **391**, 832–844 (1992).
7. D. Rabin, "A true-field magnetogram in a solar plage region," *Astrophys. J.* **390**, L103–L106 (1992).
8. S. K. Solanki, I. Rnedi, and W. Livinston, "Infrared lines as probes of solar magnetic features. II-Diagnostic capabilities of FeI15648.5 Å and 15652.9 Å," *Astron. Astrophys.* **263**, 312–322 (1992).
9. T. J. Spirock, P. R. Goode, and H. Wang, SH52H-01, AGU Meeting, Boston, (1998).
10. C. A. Gullixson, S. L. Keil, and K. S. Balasubramaniam, "Design considerations for a near infrared imaging vector magnetograph," HO-755-96, (1996).
11. M. Bass, E. W. Van Stryland, D. R. Williams, and W. L. Wolf, *Handbook of Optics*, 2nd ed., pp. 33.52–33.70 McGraw-Hill, New York (1995).
12. W. G. Driscoll and W. Vaughan, *Handbook of Optics*, pp. 7–78, McGraw-Hill, New York (1995).
13. B. Lyot, "The birefringent filter and its applications in solar physics," *Ann. Astrophys.* **7**, 31 (1944).
14. J. W. Evans, "The birefringent filter," *J. Opt. Soc. Am. A* **39**, 229–242 (1949).

Jingshan Wang is a PhD candidate in the Department of Physics at New Jersey Institute of Technology. He received his BS degree in physics from Shandong Normal University, China, in 1984, and his MS degree in physics from Peking University, China, in 1987. From 1987 to 1995, he was working on development of the multichannel birefringent filter system and a tunable birefringent filter system at Beijing Astronomical Observatory (BAO), Chinese Academy of Sciences. His interests include solar instrumentation, optical instrumental design, optical component development, and birefringent filters and optical components for fiber communications.

Haimin Wang received the BS degree from Nanjing University, China in 1982, and the PhD degree from California Institute of Technology in 1988. From 1988 to 1995, he was on the research faculty at California Institute of Technology. He joined the New Jersey Institute of Technology (NJIT) as a faculty member of the Physics Department in 1995. He is currently a professor of physics, and the Associate Director of Big Bear Solar Observatory at NJIT. His research interests have been in the areas of solar magnetic fields, solar activity, infrared solar astronomy, solar instrumentation, space weather, and high energy solar physics. He has been an author or coauthor of more than 100 refereed publications and has coedited *The Magnetic Fields and Velocity Fields of Solar Active Regions.*

Thomas J. Spirock is a PhD candidate in the Department of Electrical and Computer Engineering at the New Jersey Institute of Technology (NJIT). He received BS and MS degrees in electrical engineering from NJIT in 1992 and 1996, respectively. His interests include solar instrumentation, specifically, the development of visible light and infrared solar vector magnetographs used to study the 3-D magnetic fields on the sun that are responsible for solar activity.

Chik-Yin Lee received a Higher Diploma degree in applied science from Hong Kong Polytechnic in 1988, and his MS degree in physics from Stevens Institute of Technology, New Jersey, in 1990. His PhD degree was offered jointly by Rutgers, The State University of New Jersey, and New Jersey Institute of Technology (NJIT) in 2000. His research area is in solar physics. The work carried out at the Big Bear Solar Observatory (BBSO) includes spectral observations, image processing, and data archiving. He made use of a unique spectral drift scanning technique in the study of the dynamics of solar chromospheric fine structures. He is also interested in studies of x-rays and microwaves of solar flares. He is currently on the teaching staff at the Physics Department of the Chinese University of Hong Kong.

Nuggehalli M. Ravindra received the BS and MS degrees from Bangalore University, India, in 1974 and 1976, respectively, and the PhD degree from the University of Roorkee, India, in 1982. From 1982 to 1987, he was associated with CNRS Laboratories, Montpellier and Paris, France, the International Center for Theoretical Physics, Treste, Italy, the Microelectronics Center of North Carolina, and Vanderbitt University, Nashville. He is a professor of physics at the New Jersey Institute of Technology. His research interests have been in the areas of microelectronics, optoelectronics, process monitoring and control, temperature sensors, and related topics. He has been an author or coauthor of more than 130 refereed publications and has coedited the book *Transient Thermal Processing Techniques in Electronic Materials* [TMS, Warrendale, Philadelphia (1996)]. He has been a guest editor of the *Journal of Electronic Materials* published by TMS & IEEE and JOMe—a web-based journal published by TMS.

Jun Ma is a MS candidate in the Department of Mechanical Engineering at New Jersey Institute of Technology. His major field focuses on robotics and CAD/CAM in mechanical engineering. In this project, he was responsible for designing and manufacturing a testing system for the final filter system. Since June 2000, he is at enFashion, Inc. as a graphics programmer in the field of physical modeling. He received his BS degree in fluid mechanics from Nanjing University of Aeronautics and Astronautics, China, in 1998.

Philip R. Goode is the Director of Big Bear Solar Observatory at New Jersey Institute of Technology (NJIT). His primary research interests are the internal structure of the sun, the nature of the sun's magnetic fields, flares, coronal mass ejections, and space weather. He is also measuring and modeling the earth's reflectance from studies of earthshine and satellite cloud cover data, respectively.

Carsten Denker received the diploma and PhD in physics from the Georg-August University of Göttingen, Germany, in 1991 and 1996, respectively. In 1993, he received the diploma degree in social sciences from the Georg-August University of Göttingen. From 1989 to 1996, he was a teaching and research assistant at Universitäts-Sternwarte Göttingen. In 1992, he was a summer research assistant at the National Solar Observatory, Sacramento Peak. In 1996, he became a postdoctoral scholar in solar astrophysics at the California Institute of Technology. From 1997 to 1999, he worked as a postdoctoral research associate at the Big Bear Solar Observatory (BBSO) of the New Jersey Institute of Technology. He is currently assistant research professor at BBSO. His research interests are in solar activity, small-scale magnetic fields, 2-D spectroscopy, image reconstruction, and speckle interferometry.